

# Efficient photodegradation of paracetamol by TiO<sub>2</sub>/ZnO photocatalyst and prediction via Fuzzy Inference System

Zul Adlan Mohd Hir<sup>1,2\*</sup> , Hamizah Mokhtar<sup>3</sup> , Hartini Ahmad Rafeaie<sup>4</sup> ,  
Shaari Daud<sup>1</sup> , Norshahidatul Akmar Mohd Shohaimi<sup>1</sup> , Nik Muhammad  
Farhan Hakim Nik Badrul Alam<sup>5</sup> 

<sup>1</sup>Faculty of Applied Sciences, Universiti Teknologi MARA Pahang, 26400 Bandar Tun Abdul Razak Jengka, Pahang, Malaysia.

<sup>2</sup>Catalysis for Sustainable Water and Energy Nexus Research Group, School of Chemical Engineering, College of Engineering, Universiti Teknologi MARA, Shah Alam, Selangor, Malaysia.

<sup>3</sup>Civil Engineering Studies, College of Engineering, Universiti Teknologi MARA Pahang Branch, 26400 Jengka, Pahang, Malaysia.

<sup>4</sup>Centre of Foundation Studies, Universiti Teknologi MARA, Selangor Branch, Dengkil Campus, 43800 Dengkil, Selangor, Malaysia.

<sup>5</sup>College of Computing, Informatics and Mathematics, Universiti Teknologi MARA Pahang, 26400 Bandar Tun Abdul Razak Jengka, Pahang, Malaysia.

\*Corresponding author: [zuladlan@uitm.edu.my](mailto:zuladlan@uitm.edu.my)

## Original Research

## Abstract:

Received:  
11 January 2024  
Revised:  
25 February 2024  
Accepted:  
3 April 2024  
Published online:  
11 May 2024

© The Author(s) 2024

A facile chemical mixing approach was used to prepare TiO<sub>2</sub>/ZnO photocatalysts with different mass ratios. The photodegradation activity was tested against paracetamol in an aqueous phase assisted by low UVC-light intensity (9 W). Characterization analyses revealed that the TiO<sub>2</sub>/ZnO particles mainly exhibited irregular shapes with uniform distributions and high crystallinity degree, the primary oxidation state in the structure is titanium Ti<sup>4+</sup> of anatase TiO<sub>2</sub> (459.2 and 464.9 eV), and the presence of standard chemical state of Zn<sup>2+</sup> (1021.9 and 1044.9 eV). The composite with a 1:5 mass ratio displayed a rapid and outstanding degradation percentage of 95% and a rate of 1.83 × 10<sup>-2</sup> min<sup>-1</sup>. The best photocatalyst can be recycled up to five times towards paracetamol degradation without any regeneration step or severe deactivation. A Fuzzy inference system (FIS) was computed for the first time to investigate the relationship between the TiO<sub>2</sub>/ZnO ratio, degradation percentage, and rate constant. The optimal concentration of 9 mg/L was obtained, whereby the degradation percentage and rate were sufficiently maintained above 90% and 0.19 mg/L.min, respectively. Using a fuzzy logic controller (FLC) in this work enables future guidance and prediction for developing the best TiO<sub>2</sub>/ZnO photocatalysts for real-world water remediation processes.

**Keywords:** Fuzzy inference system; Paracetamol; Photodegradation; Titanium dioxide; Water remediation; Zinc oxide

## 1. Introduction

The penetration of pharmaceutical residues in the environment, especially water, has been a major source of anxiety among scientists. The residues commonly find their way into the water stream through sewage and wastewater treat-

ment plants, veterinary use, medical waste, and domestic waste [1]. Paracetamol, an over-the-counter medication, is an analgesic and antipyretic drug that has been effective and extensively used in medical practice. Paracetamol has been identified in surface water at 10–100 mg/L concentrations, with concentrations as high as 10 mg/L recorded in

wastewater effluents [2]. This drug is persistent and non-biodegradable due to its complex molecular structure, and it is difficult to remove using traditional water treatment processes. Indeed, the presence of paracetamol in water can have a significant adverse health effect on humans. Cancer, antibiotic resistance, endocrine disruption, and several chronic diseases may be a result of long-term exposure to paracetamol [3, 4]. Based on this fact, there is an urgent need to develop an advanced technique for effectively eliminating paracetamol from water.

The current trend to remove harmful substances from polluted water is using a heterogeneous photocatalysis approach. In this context, semiconductor oxide is widely used in photocatalysis due to its photoactivity, nontoxicity, low cost, and broad-spectrum efficacy against a wide range of organic pollutants. In general, when the photocatalyst is exposed to light irradiation with corresponding energy equal to or higher than the photocatalyst's band gap, the excitation of electrons from the valence band (VB) to the conduction band (CB) leads to the formation of the electron-hole pairs ( $e^-$  and  $h^+$ ). The holes have a high oxidation potential, and they can react with  $OH^-$  and  $H_2O$  to create  $\bullet OH$ , which takes part in the degradation process. The electrons in the CB can also produce  $\bullet O_2^-$ , which possesses an adequate reduction potential to break down organic pollutants and convert them into stable and safe compounds such as water and carbon dioxide [5, 6]. Among semiconductor metal oxides, zinc oxide (ZnO) is widely recognised as one of the most favourable photocatalytic materials for pollutant abatement in water. It possesses a 3.37 eV bandgap, strong mechanical, thermal, and chemical stability, nontoxic, inexpensive, and can absorb a large amount of the light spectrum (solar and UV)[7]. However, photo corrosion of pure ZnO produced by photoinduced holes was discovered to be significant during the reaction, potentially affecting ZnO's stability and photocatalytic activity. Its practical application is also constrained by the quick recombination of photoinduced electrons and holes [8]. Several attempts, such as metal doping [9], non-metal doping [10], and heterojunction creation [11], have been made to improve its charge separation efficiency and prevent photo corrosion.

Titanium dioxide ( $TiO_2$ ) has recently emerged as a good choice for forming heterojunctions with ZnO due to its photostability, economical, and environmentally safe with a wide bandgap of 3.20 eV that could provide a viable solution to improve charge separation [12, 13]. Previous research has revealed that the heterostructure formation and synergistic interaction of  $TiO_2$  and ZnO continue to improve photocatalytic activity. Mousa et al. demonstrated that charge transfer from the ZnO to the  $TiO_2$  surfaces occurred via heterojunction due to effective charge carrier separation at the heterojunction interfaces under direct sunlight irradiation [7]. Similarly, combining  $TiO_2$  and ZnO could provide more surface-active sites and larger surface area than single photocatalysts. As a result, numerous reactive radical species formed on the surfaces, resulting in increased photoactivity [13]. The charge recombination rate can be reduced with the appropriate band alignment, resulting in improved high electron transport and increased

photocatalytic activity. However, there has not been much research that proposes the photocatalytic performance of  $TiO_2$  via heterojunction with ZnO under a very low UV light intensity against paracetamol in the aqueous phase.

In this work,  $TiO_2/ZnO$  composite photocatalysts were prepared using a straightforward chemical mixing approach using commercially available  $TiO_2$  and ZnO nanoparticles. The composites with different ratios were prepared by simply adjusting the mass of both materials. The photocatalytic performances of the composites were tested against paracetamol in the aqueous phase under a very low UVC light intensity (9 W). The structural, functional groups, morphological features, surface compositions, and chemical state of the  $TiO_2/ZnO$  composite photocatalysts were examined by employing multitudinous characterization techniques. Recyclability tests were also carried out to assess the long-term feasibility and applicability of the prepared photocatalyst. Furthermore, a fuzzy inference system (FIS) was used for the first time to predict the degradation percentage of paracetamol by using different ratios of  $TiO_2/ZnO$  composite photocatalysts and its initial concentrations parameter. The root mean square errors (RMSE) are also computed to assess the deviation of projected findings from the experimental data. This work is expected to offer a new guide for constructing enhanced photocatalysts with promising prospects and modeling in the photocatalytic water remediation process.

## 2. Experimental

### 2.1 Materials

Titanium dioxide (particle size: 1–150 nm, 99%) and zinc oxide (particle size: 1–100 nm, 99.9%) were purchased from Sigma-Aldrich (Selangor, Malaysia). Paracetamol was acquired from a local pharmacy in Malaysia. All chemicals were utilized as received, with no purification, and deionized water was used throughout the experimental procedures.

### 2.2 Preparation of $TiO_2/ZnO$ photocatalyst

A straightforward chemical mixing method was used to prepare the  $TiO_2/ZnO$  composite photocatalysts. In brief, 0.1 g of  $TiO_2$  and 0.1 g of ZnO were mixed in 50 mL of deionized water and stirred for 1 h at room temperature. Then, the slurry mixtures were dried overnight in an oven at 80°C. Following that, the dry powder sample was grounded further to achieve a fine powder particle and labeled as 1:1. To explore the synergistic effect of  $TiO_2$  and ZnO, several mass ratios of  $TiO_2$  to ZnO were formulated under the same conditions (1:3, 1:5, 3:1, 5:1). Pure  $TiO_2$  and ZnO were also used to assess the photocatalytic performance.

### 2.3 Characterizations

A powder X-ray diffractometer (XRD6000, Shimadzu) was utilized to record the phase and crystallinity of the samples with  $CuK\alpha$  radiation ( $\lambda = 1.540$ , 30 kV, 30 mA,  $2\theta = 10-70^\circ$ ) at 2°/min scanning speed. The functional groups present in the composite photocatalysts were examined using Fourier transform infrared (FT-IR) equipped with the attenuated total reflection (ATR) accessory, between 4000 and 500  $cm^{-1}$ . Their morphological and elemental composi-

tions were also examined via scanning electron microscope with an energy-dispersive X-ray analyzer (SEM-EDX, TESCAN VEGA3). The chemical states of the samples were analyzed using a monochromatic Al  $K_{\alpha}$  X-ray source and a Kratos Axis Ultra DLD X-ray photoelectron spectrometer (XPS).

## 2.4 Photocatalytic evaluation

The photocatalytic evaluation activity was carried out in a 200 mL beaker. In a beaker containing 100 mL of a 10 mg/L paracetamol solution, a predetermined amount of the  $\text{TiO}_2/\text{ZnO}$  composite photocatalyst was added. The working solution was first stirred for 30 min without irradiation to accomplish the adsorption-desorption equilibrium. The solution was then continuously stirred for 180 min under the exposure of low-intensity UVC irradiation (9 W,  $\lambda = 254$  nm). Throughout the experiment, 5 mL samples were taken every 30 min. The remaining paracetamol concentration was determined at  $\lambda_{\text{max}} = 243$  nm using a UV-vis Spectrophotometer (PerkinElmer Lambda 35), and the degradation percentage was estimated from equation 1.

$$\text{Degradation percentage(\%)} = \frac{(C_0 - C_t)}{C_0} \times 100 \quad (1)$$

where  $C_0$  is the paracetamol's initial concentration, and  $C_t$  is the residual concentration at 30 min time intervals.

## 3. Results and Discussion

### 3.1 Surface morphological and composition analyses

The surface morphological and composition characteristics of all photocatalysts are shown in Fig. 1. The SEM image indicates that the pure  $\text{TiO}_2$  and  $\text{ZnO}$  structures mostly

exhibit irregular shapes with uniform distributions (Fig. 1 a and b). All composite photocatalysts were observed to have almost similar structures as  $\text{TiO}_2$  and  $\text{ZnO}$  and were randomly dispersed onto each other surfaces (Fig. 1 c, d, e, f, and g). The smooth surface of  $\text{TiO}_2/\text{ZnO}$  (1:5) indicates the high crystallinity of the photocatalyst sample [14], as proven by the XRD spectra in Fig. 1 c. Nonetheless, the  $\text{TiO}_2/\text{ZnO}$  composites are not clearly shown in the micrographs as there are some aggregations happen especially for the ratio of 3:1 and 5:1 (Fig. 1 f and g). There was also no significant difference in terms of the shape and particle size of the photocatalysts. Fig. 1 h (i–v) presents the  $\text{TiO}_2/\text{ZnO}$  (1:5) composite composition. The mapping images show good dispersion of the particles, which is represented by blue for Ti, red for O, and green for Zn. The data showed the presence of Ti, O, and Zn, with O and Zn having the highest atomic percentages on the photocatalyst surface at 55.93 and 37.02%, respectively, and Ti coming in second at 7.05%. The absence of other peaks in the EDX pattern and the Au peak's connection to the gold coating used for SEM image collection serves to establish the samples' purity. The atomic percentage of Ti and Zn was in accordance with the ratio of 1:5, indicating that the  $\text{TiO}_2/\text{ZnO}$  composite photocatalyst had been successfully prepared.

### 3.2 Structural, chemical state, and functional group analyses

The structural, chemical state and functional groups of the samples are presented in Fig. 2. Fig. 2(A) illustrates the XRD patterns of  $\text{TiO}_2/\text{ZnO}$  composite photocatalysts with varying mass ratios of individual oxides. The patterns confirmed that the prepared photocatalysts primarily exhibit the titanium oxide anatase phase. The peaks with  $2\theta$  values of

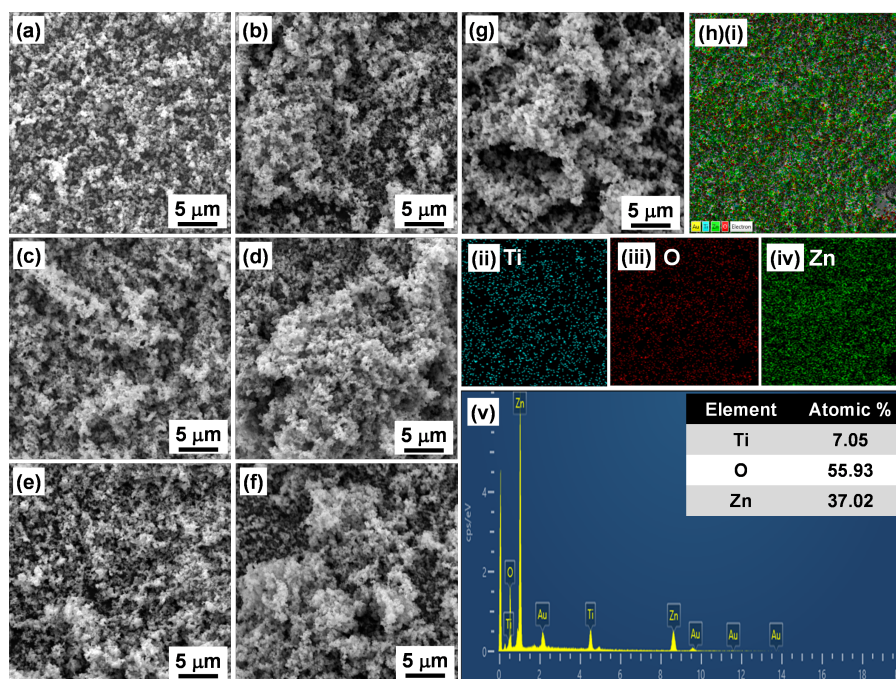


**Figure 1.** SEM images of (a) Pure  $\text{TiO}_2$ , (b) pure  $\text{ZnO}$ , (c)  $\text{TiO}_2/\text{ZnO}$  (1:1), (d)  $\text{TiO}_2/\text{ZnO}$  (1:3), (e)  $\text{TiO}_2/\text{ZnO}$  (1:5), (f)  $\text{TiO}_2/\text{ZnO}$  (3:1), (g)  $\text{TiO}_2/\text{ZnO}$  (5:1) composite photocatalysts at 5kx magnification, and (h)(i–v) elemental mapping image of  $\text{TiO}_2/\text{ZnO}$  (1:5) composite photocatalyst.

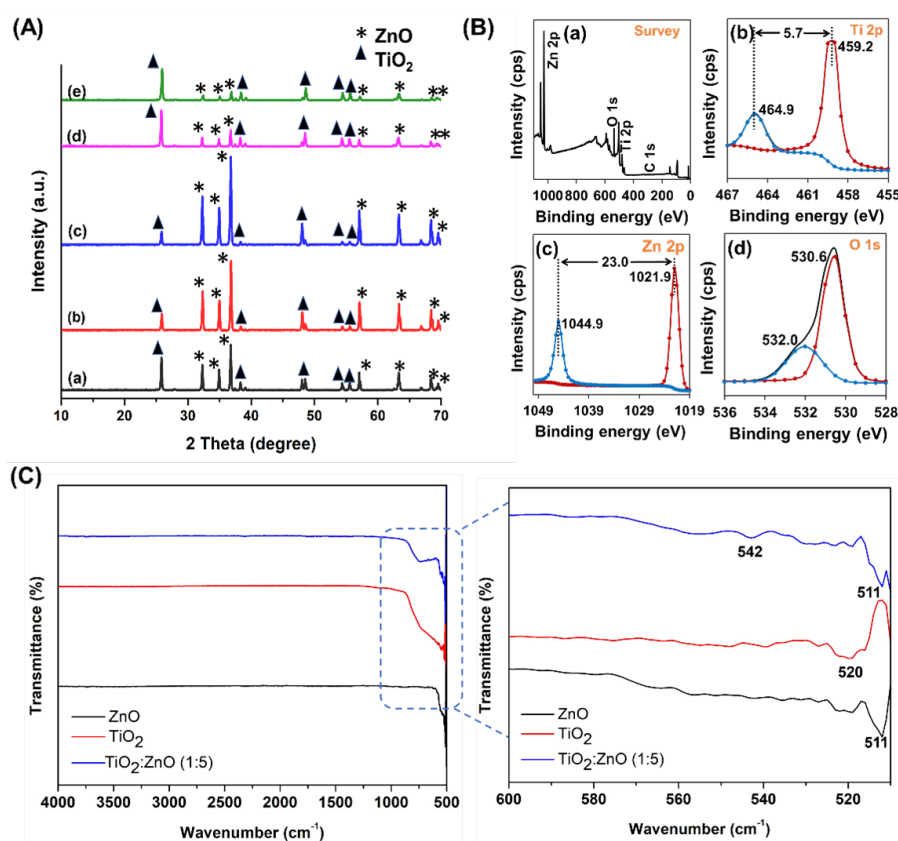


**Figure 2.** (A) XRD patterns of TiO<sub>2</sub>/ZnO composite photocatalysts at varying mass ratio of (a) 1:1, (b) 1:3, (c) 1:5, (d) 3:1 and (e) 5:1, (B) XPS analysis for (a) survey spectrum and high-resolution spectra of (b) Ti 2p, (c) Zn 2p, and (d) O 1s of TiO<sub>2</sub>/ZnO (1:5) composite photocatalyst, and (C) FTIR spectra of pure ZnO, TiO<sub>2</sub> and TiO<sub>2</sub>/ZnO (1:5) composite photocatalyst.

25.68°, 38.39°, 48.79°, 54.77° and 55.99° are corresponding to the (101), (004), (200), (105) and (211) planes, respectively, for anatase phase (JCPDS no. 75-1537) [15]. While the intense peaks observed at (100), (002), (101), (110), (110), (103), (112), and (201) planes, on the other hand, belonged to the 32.07°, 34.46°, 36.53°, 57.16°, 63.10°, 68.49° and 69.77°, respectively showing the presence of ZnO's hexagonal wurtzite structure of (JCPDS no. 75-1526)[16]. Nonetheless, increasing the TiO<sub>2</sub> content in the photocatalyst (3:1 and 5:1 ratios), the peaks corresponding to ZnO display a slight shift toward higher 2θ values. The difference in ionic radii between Zn<sup>2+</sup> (0.75 Å) and Ti<sup>4+</sup> (0.61 Å) is believed to be the cause of this shift (Fig. 1 d and e) [17, 18]. Due to prominent diffraction peaks in the spectra, the composite photocatalysts also displayed high crystallinity degrees. Moreover, no unidentified peaks were observed, suggesting that the purity of the prepared sample was consistent with the previously reported related studies [17, 19].

The XPS was utilized to understand further the surface binding energy (BE) and chemical state of the TiO<sub>2</sub>/ZnO (1:5) composite photocatalyst, as portrayed in Fig. 2 (B). The narrow scan corresponding to BE for the Ti 2p region, peaks centered at 459.2 and 464.9 eV, were attributed to Ti 2p<sub>3/2</sub> and Ti 2p<sub>1/2</sub> orbitals (Fig. 2 (B)b). The splitting between the two peaks is 5.7 eV, suggesting that the primary oxidation state in the structure is titanium Ti<sup>4+</sup> of anatase TiO<sub>2</sub>

[20]. Meanwhile, the spectrum for Zn 2p was fitted into two peaks at BE of 1021.9 (Zn 2p<sub>1/2</sub>) and 1044.9 eV (Zn 2p<sub>3/2</sub>) (Fig. 2 (B)c). The difference between the two binding energies (23 eV) was consistent with the standard chemical state of Zn<sup>2+</sup> [21]. The spectrum of O 1s was deconvoluted into two individual component peaks (Fig. 2 (B)d). The BE at 530.6 eV could be ascribed to the lattice oxygen in TiO<sub>2</sub> and ZnO for surface Ti-O-Ti and Zn-O-Zn bonds, respectively. The latter peak at 532.0 eV was consigned to chemisorbed or surface hydroxyl bonding of Ti-OH and Zn-OH [22]. Overall, the BE for TiO<sub>2</sub>/ZnO composite is slightly different due to shifting to higher values than the reported value for pure TiO<sub>2</sub> and ZnO. This was credited to the cohesive electronic transport and effective interaction between TiO<sub>2</sub> and ZnO [23].

The molecular structures of the resulting samples of pure ZnO, TiO<sub>2</sub>, and 1:5 TiO<sub>2</sub>/ZnO composite photocatalysts were analysed using FTIR spectroscopy in the range of 4000 to 500 cm<sup>-1</sup>, and the findings are portrayed in Fig. 2 (C). The spectra provided crucial details regarding the materials' bonding properties. In the case of pure ZnO, a prominent peak at 511 cm<sup>-1</sup> was observed. This peak corresponds to the Zn-O stretching vibrations, which confirm the existence of Zn-O bonding in the crystal lattice structure [24]. Meanwhile, a peak at 520 cm<sup>-1</sup> was identified to be the bending vibrations of Ti-O-Ti linkages within the TiO<sub>2</sub>

crystal lattice [25]. The presence of this peak confirms the characteristic bonding arrangement of Ti and O atoms in  $\text{TiO}_2$ . Meanwhile, with the coupling of  $\text{TiO}_2$  and ZnO at a 1:5 ratio, the spectrum displays characteristic peaks associated with both ZnO and  $\text{TiO}_2$ . A peak at  $511\text{ cm}^{-1}$  is assigned to the Zn-O stretching vibrations, while a peak at  $542\text{ cm}^{-1}$  corresponds to the Ti-O bending vibrations [26]. These peaks reflect the existence of Zn-O and Ti-O bonds within the composite, indicating the cohesive interaction of ZnO and  $\text{TiO}_2$  phases.

### 3.3 Photocatalytic evaluation

Prior to the photodegradation process, the calibration curve of the paracetamol in the aqueous phase was performed.

The calibration curve was generated using 5 to 25 mg/L of paracetamol concentrations. After the degradation process was completed, the absorbance of each sample was assessed to estimate the concentration that remained as well as the degradation percentage (Fig. 3). Fig. 3 portrays the photocatalytic degradation of paracetamol by pure  $\text{TiO}_2$ , pure ZnO, and  $\text{TiO}_2/\text{ZnO}$  composite photocatalysts with various mass ratios. According to preliminary experiments, paracetamol adsorption (under dark conditions) on  $\text{TiO}_2$  was about 19%, compared to 14% on ZnO. The fact that paracetamol was not degraded throughout the photolysis process shows that the drug is resistant to UV light irradiation, and the result is insignificant. Pure ZnO demonstrates a 1.23 times higher degradation

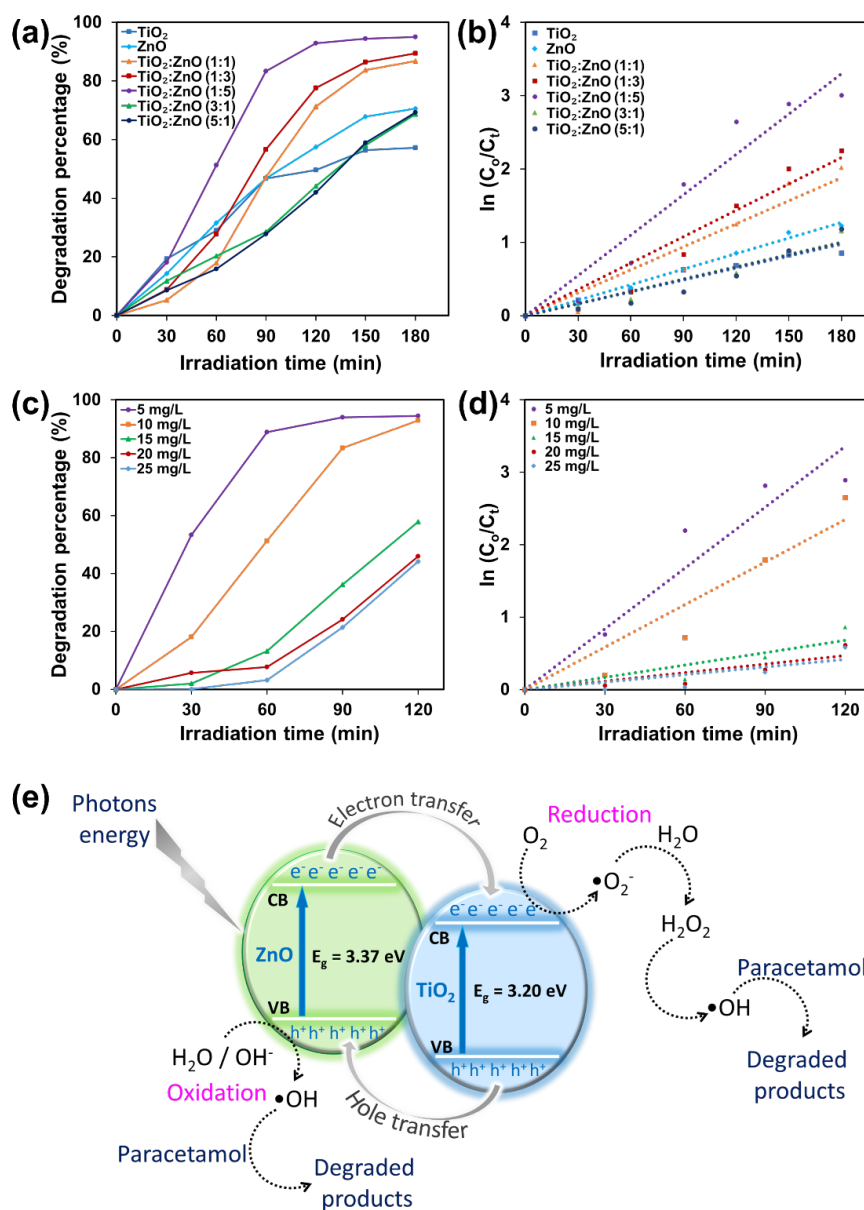


**Figure 3.** (a) Degradation percentage, (b) kinetic of paracetamol degradation by  $\text{TiO}_2/\text{ZnO}$  photocatalysts with different mass ratio, (c) degradation percentage, (d) kinetic of paracetamol degradation at different initial concentration by  $\text{TiO}_2/\text{ZnO}$  (1:5) composite photocatalyst, and (e) plausible mechanism for photodegradation of paracetamol. [Paracetamol] = 10 mg/L, pH = 6.8, mass = 0.2 g.

**Table 1.** Degradation percentage and kinetics by using different ratios of TiO<sub>2</sub>/ZnO composite photocatalysts.

Photocatalyst	Degradation percentage (%)	k <sub>obs</sub> (min <sup>-1</sup> )	Rate (mg/L.min)	Correlation factor R <sup>2</sup>
TiO <sub>2</sub>	57.22	0.0054	0.054	0.9833
ZnO	70.58	0.0071	0.071	0.9967
TiO <sub>2</sub> :ZnO (1:1)	86.77	0.0105	0.105	0.9549
TiO <sub>2</sub> :ZnO (1:3)	89.45	0.0120	0.120	0.9720
TiO <sub>2</sub> :ZnO (1:5)	95.05	0.0183	0.183	0.9789
TiO <sub>2</sub> :ZnO (3:1)	68.65	0.0056	0.056	0.9719
TiO <sub>2</sub> :ZnO (5:1)	69.31	0.0055	0.055	0.9569

percentage than TiO<sub>2</sub> (57%) in 180 min. The TiO<sub>2</sub>/ZnO composite displayed a better degradation percentage than pure photocatalysts in degrading paracetamol (Table 1). Interestingly, incorporating TiO<sub>2</sub>/ZnO with ratios of 1:1, 1:3, and 1:5 enhanced the photocatalytic performance, and the degradation rate with a ratio of 1:5 was found to be the best, with a maximum degradation percentage of 95%. This was attributed to the enhancement in the available active sites and uniform particle dispersion of ZnO on the surface of TiO<sub>2</sub>, which was sufficient for paracetamol degradation. Similarly, Zyoude et al. reported that ZnO shows better degradation efficiency than TiO<sub>2</sub> due to the higher photon absorption ability and surface area, smaller particle size, and increase in the number of available active sites [27].

The strong and synergistic interaction between TiO<sub>2</sub> and ZnO is also credited with photocatalytic improvement via a typical type-II heterojunction. Type-II heterojunction photocatalysts have an extensive light-absorption range, rapid mass transfer, and effective electron-hole separation efficiency [28, 29]. Since the two semiconductor oxides may both be photoexcited by UV irradiation to produce electron-hole pairs, there are two possible routes for interfacial charge accumulation in TiO<sub>2</sub>/ZnO surfaces. Accordingly, the CB and the VB levels of ZnO are higher than the corresponding levels of TiO<sub>2</sub>. Thus, the photogenerated electrons will transfer to TiO<sub>2</sub>, while the photogenerated holes will migrate to ZnO under light irradiation, resulting in spatial separation of electron-hole pairs, subsequently avoiding charge recombination (Fig. 3e). Through a series of redox reactions, more charge carriers are produced such as •OH and •O<sub>2</sub><sup>-</sup> radicals for efficient paracetamol degradation. The positive holes (h<sup>+</sup>) can also play a crucial role in paracetamol degradation by direct reaction with adsorbed water to produce •OH radicals.

Interestingly, the use of UVC irradiation in this work also helps in the production of more •OH species by directly splitting hydrogen peroxide in the working solution, as compared to UVA and UVB irradiations, where they cannot decompose hydrogen peroxide to hydroxyl radicals. This observation was consistent with the previously reported study [30]. The degradation percentage and rate, however, decreased significantly at a higher TiO<sub>2</sub> content (ratio 3:1 and 5:1). The effectiveness of TiO<sub>2</sub>/ZnO composite photocatalyst may vary due to higher concentration of ZnO, which increased the number of surface-active sites available for photodegradation. The photocatalyst surface with more active sites offers enhanced photons energy absorption from UV light irradiation, thereby enhancing the paracetamol degradation activity. Moreover, the higher degradation percentage can be attributed to the natural properties of ZnO, such as broad bandgap (3.37 eV), allowing it to absorb a wide range of UV light and thus facilitate efficient photoexcitation of electron-hole pairs, large exciton binding energy (60 meV) at room temperature, which can demonstrate the semiconductive and piezoelectric properties, and excellent stability [31, 32]. This stability ensures that ZnO remains active throughout the photocatalysis process, allowing it to maintain its high degradation percentage over time. Meanwhile, the presence of higher TiO<sub>2</sub> content might induce agglomeration behavior, as can be seen in Fig. 3f and g, thus reducing the available surface area and photocatalyst absorption efficiency. These results revealed that there was a limit to how much TiO<sub>2</sub> and ZnO could be added without compromising the overall photocatalytic performance. On the basis of the overall photocatalytic performances, the optimal mass ratio of TiO<sub>2</sub>/ZnO (1:5) composite photocatalyst was utilized to evaluate the influence of the initial concentration of paracetamol. The degradation

**Table 2.** Degradation percentage and kinetics at different initial concentrations using the TiO<sub>2</sub>/ZnO (1:5) composite photocatalyst.

Paracetamol concentration (mg/L)	Degradation percentage (%)	k <sub>obs</sub> (min <sup>-1</sup> )	Rate (mg/L.min)	Correlation factor R <sup>2</sup>
5	94.47	0.0280	0.140	0.9735
10	92.92	0.0196	0.196	0.9585
15	57.80	0.0057	0.086	0.8970
20	45.99	0.0039	0.078	0.8826
25	44.14	0.0035	0.088	0.8135

percentage decreased as the concentration rose from 5 to 25 mg/L within 120 min of irradiation (Table 2), as depicted in Fig. 3c and d. The decrease in the degradation percentage might be attributed to several reasons. Firstly, a higher concentration of paracetamol may occupy a greater number of TiO<sub>2</sub>/ZnO active sites by competing with •OH for the adsorption onto the catalyst surface, subsequently suppressing the formation of photogenerated charge carriers and resulting in lower degradation rates. Secondly, the abundant paracetamol molecule may also function as a barrier, preventing photons from reaching the catalytic surface. Thirdly, a higher paracetamol concentration absorbs more photons, reducing the number of photons necessary to activate TiO<sub>2</sub>/ZnO. The scarcity of photons to activate the TiO<sub>2</sub>/ZnO surface essentially retarded the photodegradation activity. A similar observation was also reported from a previous study when working with concentrated paracetamol using barium ferrate via bismuth and copper co-doping (Ba<sub>1-x</sub>Bi<sub>x</sub>Fe<sub>1-x</sub>Cu<sub>x</sub>O<sub>3</sub>) photocatalyst [33]. All conditions limit the formation of radical species required for paracetamol breakdown; therefore, the formation of radicals is insufficient to eliminate the highly concentrated contaminant. Since the amount of catalyst used is also fixed, generating reactive radical species would also be limited, reducing the catalyst's ability to degrade. Another factor that may reduce degradation efficiency is competition for photogenerated radicals among adsorbed paracetamol, chemical intermediates, and water molecules [34].

Given the affinity of •OH for electron-rich aromatic molecules, it is hypothesized that the breakdown occurred by further hydroxylation and oxidation of phenolic compounds [35]. The hydroxylation of the benzene ring results in the production of 3-hydroxyacetaminophen, 4-aminophenol, hydroquinone, 1,4-benzoquinone, and acetamide [36–39]. However, continued oxidation of the intermediates could cause the aromatic structure to break, resulting in the conversion to acids, carbon dioxide, and water molecules.

The following equations represent the Langmuir–Hinshelwood (L-H) kinetic model, which was used to analyse the degradation kinetics [40].

$$r = -\left(\frac{dC}{dt}\right) = k_{obs}C \quad (2)$$

$$\ln\left(\frac{C_0}{C_t}\right) = k_{obs}t \quad (3)$$

where  $r$  is the reaction rate,  $k_{obs}$  is the rate constant (min<sup>-1</sup>),  $C_0$  is the paracetamol's initial concentration and  $C_t$  is the residual concentration at 30 min time interval.

The paracetamol degradation followed pseudo-first-order kinetics, as seen in Figures 3 b and d. The TiO<sub>2</sub>/ZnO (1:5) composite photocatalyst had the highest rate constant of  $1.83 \times 10^{-2} \text{ min}^{-1}$  and, consequently, the highest rate of paracetamol degradation, in accordance with the degradation percentage.

### 3.4 Prediction Using Fuzzy Inference System

The fuzzy inference system (FIS) is a fuzzy logic system that converts numerical data into linguistic terms and pro-

cesses the information based on several fuzzy logic rules before being converted back into numerical forms. Converting the numerical values into linguistic terms is called fuzzification. Meanwhile, the reverse activity to obtain the final numerical values is known as defuzzification. Basically, the FIS consists of three main parts: fuzzification, fuzzy inference engine, and defuzzification [41]. In this research, the FIS was applied to predict the degradation percentage and rate when using different TiO<sub>2</sub>/ZnO composite photocatalysts (Fig. 4).

Fig. 4(A) illustrates the developed FIS with two input and two output variables. For each variable, five linguistic terms are used to fuzzify the data: “very low,” “low,” “medium,” “high,” and “very high.” These linguistic terms are characterized by the Gaussian membership function, estimated using equation 4.

$$\mu(x) = \frac{1}{\sqrt{2\pi}\sigma} \exp\left(-\frac{(x-m)^2}{2\sigma^2}\right) \quad (4)$$

where  $\sigma$  and  $m$  are the standard deviation and mean, respectively. The Gaussian membership function is used instead of triangular or trapezoidal membership functions due to its supremacy in obtaining better-predicted results [42]. Fig. 4 (B) displays the membership functions which characterize the linguistic terms for each input and output variable.

Next, the fuzzy logic rules are then constructed to allow the rule-guided prediction of the degradation percentage and rate. The following five rules are used to perform such prediction using the FIS:

1. If (Ratio-TiO<sub>2</sub> is very low) and (Ratio-ZnO is very low), then (Degradation is high) (Rate is medium).
2. If (Ratio-TiO<sub>2</sub> is very low) and (Ratio-ZnO is medium), then (Degradation is high) (Rate is medium).
3. If (Ratio-TiO<sub>2</sub> is very low) and (Ratio-ZnO is very high), then (Degradation is very high) (Rate is very high).
4. If (Ratio-TiO<sub>2</sub> is medium) and (Ratio-ZnO is very low), then (Degradation is low) (Rate is low).
5. If (Ratio-TiO<sub>2</sub> is very high) and (Ratio-ZnO is very low), then (Degradation is low) (Rate is low).

As a result, generating the FIS leads to the prediction of the degradation percentage and rate, as illustrated in Fig. 4(C). The three-dimensional surfaces were obtained, with each indicating the degradation percentage and rate when various TiO<sub>2</sub> and ZnO ratios were utilized. Since this work used five combinations of TiO<sub>2</sub>/ZnO ratios, as displayed in Table 1, the developed FIS allows the prediction of other combinations of TiO<sub>2</sub>/ZnO ratios, such as 3:3, 3:5, and others.

As 1:5 was identified as the optimal mass ratio of TiO<sub>2</sub>/ZnO composite photocatalyst as displayed in Table 1, another FIS is developed to predict the effect of different initial concentrations of paracetamol on the degradation percentage and rate using the TiO<sub>2</sub>/ZnO (1:5) composite photocatalyst (Fig. 5). The FIS displayed in Fig. 5(A) shows one input variable and two output variables. Analogous to the previous FIS, five linguistic terms were used to fuzzify the variables, and the Gaussian membership functions were implemented to characterize the linguistic terms. Fig. 5(B) presents the Gaussian membership functions for each variable.

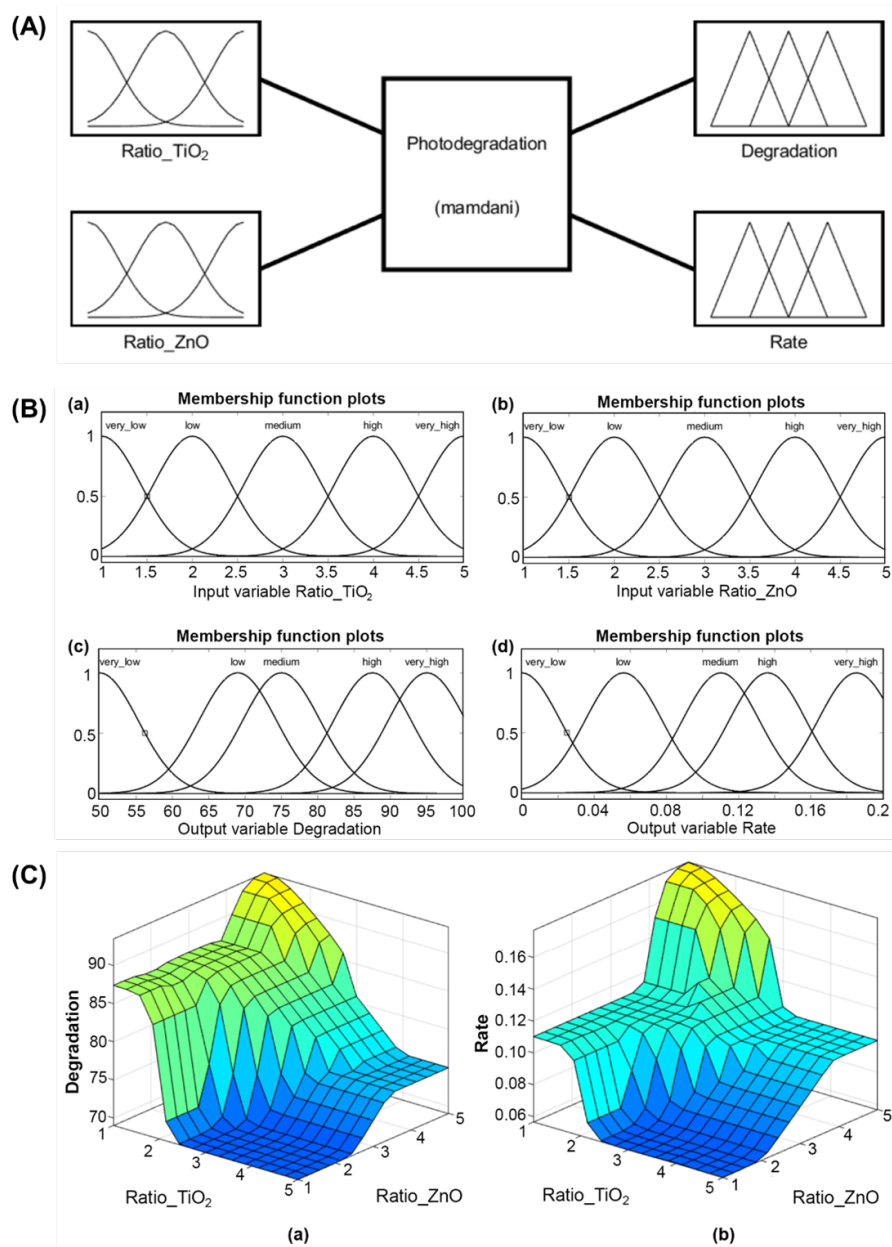


**Figure 4.** (A) Fuzzy inference system of the photodegradation using different TiO<sub>2</sub>/ZnO composite photocatalysts, (B) Membership functions of the input and output variables for the photodegradation using different TiO<sub>2</sub>/ZnO composite photocatalysts (a) ratio of TiO<sub>2</sub>, (b) ratio of ZnO, (c) degradation percentage, (d) degradation rate, and (C) Predicted curves using different ratios of TiO<sub>2</sub>/ZnO composite photocatalysts (a) degradation percentage, and (b) degradation rate.

In this FIS, five fuzzy logic rules are used to predict the degradation percentage and rate. The constructed rules are as follows:

- 1.If (Paracetamol concentration is very low), then (Degradation percentage is very high) (Rate is medium).
- 2.If (Paracetamol concentration is low), then (Degradation percentage is very high) (Rate is very high).
- 3.If (Paracetamol concentration is medium), then (Degradation percentage is medium) (Rate is very low).
- 4.If (Paracetamol concentration is high), then (Degradation percentage is low) (Rate is very low).
- 5.If (Paracetamol concentration is very high), then (Degradation percentage is low) (Rate is low).

Based on the predicted results of the developed FIS, the

optimal paracetamol concentration is obtained as 9 mg/L (Fig. 5(C)). The degradation percentage and rate are maintained above 90% and 0.19 mg/L.min, respectively. Hence, the predicted concentration of 9 mg/L can be considered when future photodegradation activity is going to be conducted on a larger scale. Table 3 compares the predicted and experimental results of the degradation percentage and rate when different paracetamol concentrations are used. Furthermore, the root mean square errors (RMSE) were calculated to measure the deviation of the predicted results from the experimental data, and they are obtained as 2.9310 and 0.0023 for the degradation percentage and rate, respectively. With the minimized errors produced by the developed FIS, the predicted results are still reliable compared to the exper-

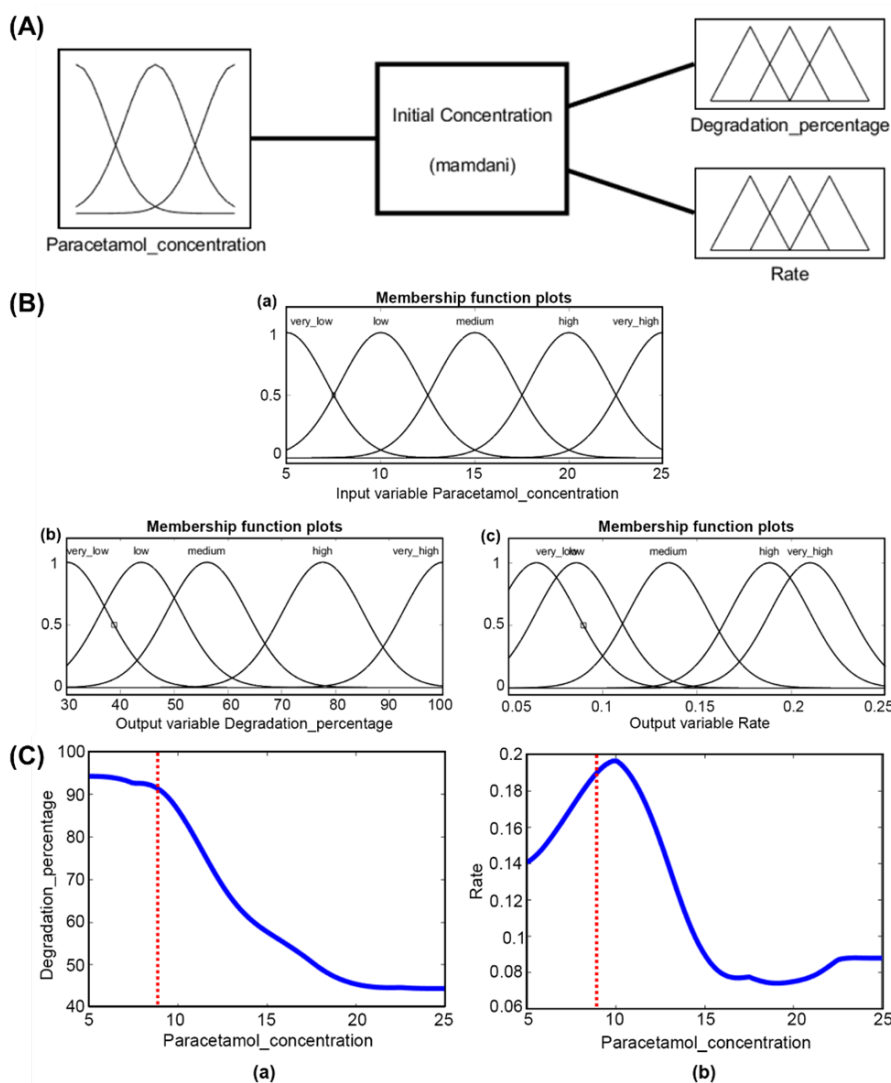


**Figure 5.** (A) Fuzzy inference system of the photodegradation using different initial concentrations of paracetamol, (B) Membership functions of the input and output variables of (a) paracetamol concentration, (b) degradation percentage, (c) rate, and (C) Prediction of photodegradation performance using different initial concentrations of paracetamol with (a) degradation percentage, and (b) degradation rate by the TiO<sub>2</sub>/ZnO (1:5) composite photocatalyst.

imental results. In fact, the FIS allows the prediction of the output when there is a lack of information. For example, the FIS can predict the degradation percentage and rate when a specific paracetamol concentration between 5 and 10 mg/L is used. The FIS unveils the uncertainty and serves as a flexible model which adapts to process changes [43].

### 3.5 Recyclability

The recyclability of the best composite photocatalyst (TiO<sub>2</sub>/ZnO (1:5)) for paracetamol degradation was further explored by pouring in fresh paracetamol aqueous phase (10 mg/L) into the new reaction cycle without undergoing any regeneration procedure (Fig. 6). Noticeably, the photocatalyst exhibited high degradation activity, with more than 75% of degradation percentage after five consecutive

**Table 3.** Experimental and predicted degradation percentage and rate using different paracetamol concentration.

Paracetamol concentration (mg/L)	Degradation percentage (%)		Rate (mg/L.min)	
	Experimental	Predicted	Experimental	Predicted
5	94.47	94.30	0.1400	0.1410
10	92.92	86.40	0.1960	0.1970
15	57.80	57.80	0.0860	0.0899
20	45.99	45.99	0.0780	0.0750
25	44.14	44.14	0.0880	0.0879

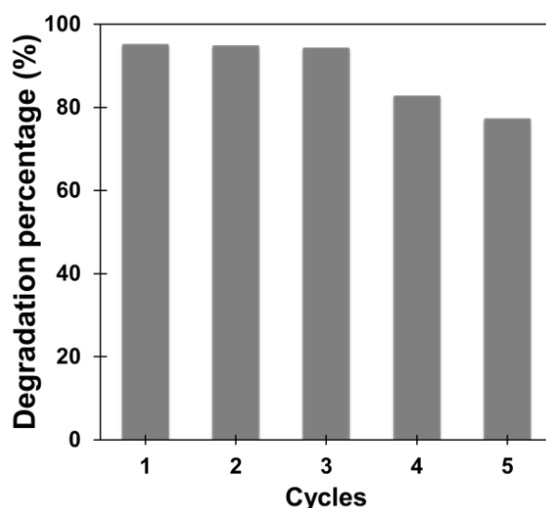


**Figure 6.** Recyclability test of the TiO<sub>2</sub>/ZnO (1:5) composite photocatalyst. [Paracetamol] = 10 mg/L, pH = 6.8, mass = 0.2 g.

cycles. The decline in the degradation percentage could be due to the loss of the catalyst sample during the filtration process. Nonetheless, the result demonstrates the stability of the TiO<sub>2</sub>/ZnO composites in the paracetamol degradation against UVC irradiation and has a high potential for the photocatalytic wastewater remediation process.

#### 4. Conclusion

The TiO<sub>2</sub>/ZnO composite photocatalysts were successfully prepared via a simple mixing approach. The TiO<sub>2</sub>/ZnO particles had irregular shapes, uniform distributions, and high degrees of crystallinity, with titanium Ti<sup>4+</sup> of anatase TiO<sub>2</sub> being the primary oxidation state in the structure and Zn<sup>2+</sup> being present in its standard chemical state. The composite with a mass ratio of 1:5 demonstrated 95% paracetamol degradation at a rate of  $1.83 \times 10^{-2} \text{ min}^{-1}$ , in accordance with pseudo-first-order kinetics. The enhanced photocatalytic performance was credited to the effective charge separation, ease of migration of electrons, high dispersity of ZnO on the surface of TiO<sub>2</sub>, and increased number of available active sites. The fuzzy inference system (FIS) was computed to predict the photodegradation activity of the TiO<sub>2</sub>/ZnO composite prepared by different ratios and initial concentrations of paracetamol. The optimal concentration of 9 mg/L was identified using fuzzy logical rules, in which the degradation percentage and rate were sufficiently maintained above 90% and 0.19 mg/L.min, respectively. The deviation of the predicted findings from the experimental data was found to be 2.9310 and 0.0023 for the degradation percentage and rate, respectively. Overall, the best composite photocatalyst was stable against low-intensity UVC irradiation and performed well for up to 5 cycles without undergoing any regeneration procedure.

#### Acknowledgments

This research was funded by University Teknologi MARA (UiTM) Pahang Branch, Malaysia, under the GT2P Grant (Project Number: 600-TNCPI 5/3/DDN (06) (014/2023))

and MyRA LPhD Grant (Project number: 600-RMC/GPM LPHD 5/3 (166/2021)). The authors thank the services and facilities provided by UiTM Pahang Branch and UiTM Shah Alam to carry out the laboratory work.

#### Authors Contributions

All authors have contributed equally to prepare the paper.

#### Availability of Data and Materials

The data that support the findings of this study are available from the corresponding author upon reasonable request.

#### Conflict of Interests

The authors declare that they have no known competing financial interests or personal relationships that could have appeared to influence the work reported in this paper.

#### Open Access

This article is licensed under a Creative Commons Attribution 4.0 International License, which permits use, sharing, adaptation, distribution and reproduction in any medium or format, as long as you give appropriate credit to the original author(s) and the source, provide a link to the Creative Commons license, and indicate if changes were made. The images or other third party material in this article are included in the article's Creative Commons license, unless indicated otherwise in a credit line to the material. If material is not included in the article's Creative Commons license and your intended use is not permitted by statutory regulation or exceeds the permitted use, you will

need to obtain permission directly from the OICC Press publisher. To view a copy of this license, visit <https://creativecommons.org/licenses/by/4.0>.

## References

- [1] M. Magureanu, N.B. Mandache, and V.I. Parvulescu. *Water Res*, **81** (2015):124–136. DOI: <https://doi.org/10.1016/j.watres.2015.05.037>.
- [2] P.T. Lum, K.Y. Foo, and N.A. Zakaria. *Malaysian J. Anal. Sci*, **23** (2019):771–780. DOI: <https://doi.org/10.17576/mjas-2019-2305-02>.
- [3] E. Brillas and J. Manuel Peralta-Hernandez. *Sep. Purif. Technol*, **309** (2023):122982. DOI: <https://doi.org/10.1016/j.seppur.2022.122982>.
- [4] S.Y. Wee and A.Z. Aris. *Environ. Int*, **106** (2017):207–233. DOI: <https://doi.org/10.1016/j.envint.2017.05.004>.
- [5] M. Asri, A. Naghizadeh, A. Hasani, S. Mortazavi, A. Javid, and F. Masoud. *AQUA — Water Infrastructure, Ecosyst. Soc*, **72** (2023):1800–1814. DOI: <https://doi.org/10.2166/aqua.2023.313>.
- [6] K. Sharma, V. Hasija, M. Malhotra, P.K. Verma, A.A. Parwaz Khan, S. Thakur, Q. Van Le, H.H. Phan Quang, V.-H. Nguyen, P. Singh, and P. Raizada. *Int. J. Hydrogen Energy*, **52** (2024):804–818. DOI: <https://doi.org/10.1016/j.ijhydene.2023.09.033>.
- [7] H.M. Mousa, J.F. Alenezi, I.M.A. Mohamed, A.S. Yasin, A.F.M. Hashem, and A. Abdal-hay. *J. Alloys Compd*, **886** (2021):161169. DOI: <https://doi.org/10.1016/j.jallcom.2021.161169>.
- [8] K.M. Lee, C.W. Lai, K.S. Ngai, and J.C. Juan. *Water Res*, **88** (2016):428–448. DOI: <https://doi.org/10.1016/j.watres.2015.09.045>.
- [9] Z. Warren, J. Wenk, and D. Mattia. *RSC Adv*, **13** (2023):2438–2450. DOI: <https://doi.org/10.1039/D2RA06730G>.
- [10] V. Kumari, A. Mittal, J. Jindal, S. Yadav, and N. Kumar. *Front. Mater. Sci.*, **13** (2019):1–22. DOI: <https://doi.org/10.1007/s11706-019-0453-4>.
- [11] L. Yu, W. Chen, D. Li, J. Wang, Y. Shao, M. He, P. Wang, and X. Zheng. *Appl. Catal. B Environ*, **164** (2015):453–461. DOI: <https://doi.org/10.1016/j.apcatb.2014.09.055>.
- [12] Q. Jiang, Z. Han, Y. Yuan, C. Cai, J. Li, and Z. Cheng. *Mater. Chem. Phys.*, **279** (2022):125737. DOI: <https://doi.org/10.1016/j.matchemphys.2022.125737>.
- [13] P. Akhter, S. Nawaz, I. Shafiq, A. Nazir, S. Shafique, F. Jamil, Y.K. Park, and M. Hus-sain. *Mol. Catal*, **535** (2023):112896. DOI: <https://doi.org/10.1016/j.mcat.2022.112896>.
- [14] M. Hou, J. Gao, L. Yang, S. Guo, T. Hu, and Y. Li. *Appl. Surf. Sci*, **535** (2021):147666. DOI: <https://doi.org/10.1016/j.apsusc.2020.147666>.
- [15] A. Zatirostami. *Mater. Today Commun*, **26** (2021):102033. DOI: <https://doi.org/10.1016/j.mtcomm.2021.102033>.
- [16] G.K. Upadhyay, J.K. Rajput, T.K. Pathak, V. Kumar, and L.P. Purohit. *Vacuum*, **160** (2019):154–163. DOI: <https://doi.org/10.1016/j.vacuum.2018.11.026>.
- [17] M.M. Ali, M.J. Haque, M.H. Kabir, M.A. Kaiyum, and M.S. Rahman. *Results Mater*, **11** (2021):100199. DOI: <https://doi.org/10.1016/j.rinma.2021.100199>.
- [18] W. Shu-qin, L.I. Xiao-xue, and L.I. Dan. *J. Fuel Chem. Technol.*, **51** (2023):589–598. DOI: [https://doi.org/10.1016/S1872-5813\(22\)60070-7](https://doi.org/10.1016/S1872-5813(22)60070-7).
- [19] K. Kighuta, A.I. Gopalan, D.E. Lee, G. Saianand, Y.L. Hou, S.S. Park, K.P. Lee, J.C. Lee, and W.J. Kim. *J. Environ. Chem. Eng.*, **9** (2021):106417. DOI: <https://doi.org/10.1016/j.jece.2021.106417>.
- [20] Y. Liu, H. Yao, L. Wu, Z.-H. Xie, and C.-J. Zhong. *Appl. Surf. Sci*, **614** (2023):156109. DOI: <https://doi.org/10.1016/j.apsusc.2022.156109>.
- [21] M. Hatzisymeon, M.K. Daletou, G. Ras-sias, and C.A. Aggelopoulos. *Sep. Purif. Technol*, **320** (2023):124119. DOI: <https://doi.org/10.1016/j.seppur.2023.124119>.
- [22] X. Zheng, D. Li, X. Li, J. Chen, C. Cao, J. Fang, J. Wang, Y. He, and Y. Zheng. *Appl. Catal. B Environ*, **168–169** (2015):408–415. DOI: <https://doi.org/10.1016/j.apcatb.2015.01.001>.
- [23] X. An, B. Zhang, C. Wang, Z. Zhao, S. Zhang, H. Bala, and Z. Zhang. *J. Mater.*, **9** (2023):725–734. DOI: <https://doi.org/10.1016/j.jmat.2023.01.013>.
- [24] G.R.S. Andrade, C.C. Nascimento, Z.M. Lima, E. Teixeira-Neto, L.P. Costa, and I.F. Gimenez. *Appl. Surf. Sci.*, **399** (2016):573–582. DOI: <https://doi.org/10.1016/j.apsusc.2016.11.202>.
- [25] S. Silvestri, T.A.L. Burgo, C. Dias-Ferreira, J.A. Labrincha, and D.M. Tobaldi. *React. Funct. Polym*, **146** (2020):104401. DOI: <https://doi.org/10.1016/j.reactfunctpolym.2019.104401>.
- [26] C. Cheng, A. Amini, C. Zhu, Z. Xu, H. Song, and N. Wang. *Sci. Rep*, **4** (2014):4181. DOI: <https://doi.org/10.1038/srep04181>.
- [27] A.H. Zyoud, A. Zubi, S. Hejjawi, S.H. Zyoud, M.H. Helal, S.H. Zyoud, N. Qamhieh, A.R. Hajamohideen, and H.S. Hilal. *J. Environ. Chem. Eng*, **8** (2020):104038. DOI: <https://doi.org/10.1016/j.jece.2020.104038>.

- [28] J. Low, J. Yu, M. Jaroniec, S. Wageh, and A.A. Al-Ghamdi. *Adv. Mater.*, **29** (2017):1601694. DOI: <https://doi.org/10.1002/adma.201601694>.
- [29] S. San Martln, M.J. Rivero, and I. Ortiz. *Catalysts*, **10** (2020):901. DOI: <https://doi.org/10.3390/catal10080901>.
- [30] A.R. Khataee and M. Zarei. *Desalination*, **273** (2011):453–460. DOI: <https://doi.org/10.1016/j.desal.2011.01.066>.
- [31] T. Chankhanittha, J. Watcharakitti, V. Piyavarakorn, B. Johnson, R.J. Bushby, C. Chuaicham, K. Sasaki, S. Nijpanich, H. Nakajima, N. Chanlek, and S. Nanan. *J. Phys. Chem. Solids*, **179** (2023):111393. DOI: <https://doi.org/10.1016/j.jpcs.2023.111393>.
- [32] Z.A.M. Hir, N.M.F.H.N.B. Alam, A.So. Shaari, and H.A. Rafaie. *Malaysian J. Chem.*, **24** (2022):37–46.
- [33] H.A. Abbas, R.A. Nasr, R.N. Vannier, and T.S. Jamil. *J. Environ. Sci.*, **112** (2022):331–342. DOI: <https://doi.org/10.1016/j.jes.2021.05.008>.
- [34] O.F.S. Khasawneh, P. Palaniandy, P. Palaniandy, M. Ahmadipour, H. Mohammadi, and M.R. Bin Hamdan. *J. Environ. Chem. Eng.*, **9** (2021):104921. DOI: <https://doi.org/10.1016/j.jece.2020.104921>.
- [35] M.O. Chijioke-Okere, Z.A. Mohd Hir, C.E. Ogukwe, P.C. Njoku, A.H. Abdullah, and E.E. Oguzie. *J. Mol. Liq.*, **338** (2021):116692. DOI: [10.1016/j.molliq.2021.116692](https://doi.org/10.1016/j.molliq.2021.116692).
- [36] E. Moctezuma, E. Leyva, C.A. Aguilar, R.A. Luna, and C. Montalvo. *J. Hazard. Mater.*, **243** (2012):130–138. DOI: <https://doi.org/10.1016/j.jhazmat.2012.10.010>.
- [37] L. Yang, L.E. Yu, and M.B. Ray. *Environ. Sci. Technol.*, **43** (2009):460–465. DOI: <https://doi.org/10.1021/es8020099>.
- [38] M. Chijioke-Okere, A.H. Abdullah, Z.A. Mohd Hir, J.I. Alinnor, and E.E. Oguzie. *Inorg. Chem. Commun.*, **148** (2023):110377. DOI: <https://doi.org/10.1016/j.inoche.2022.110377>.
- [39] V.H.T. Thi and B.K. Lee. *Mater. Res. Bull.*, **96** (2017):171–182. DOI: <https://doi.org/10.1016/j.materresbull.2017.04.028>.
- [40] H. Mukhair, A.H. Abdullah, Z.A.M. Hir, N.S. Osman, Z. Zainal, and L. Hong Ngee. *J. Mol. Liq.*, **376** (2023):121494. DOI: <https://doi.org/10.1016/j.molliq.2023.121494>.
- [41] N. Sabri, S.A. Aljunid, M.S. Salim, R.B. Badlishah, R. Kamaruddin, and M.F. Abd Malek. *Int. Rev. Autom. Control.*, **6** (2013):441–449.
- [42] S. Chatterjee and A. Das. *Soft Comput.*, **24** (2020): 11731–11754. DOI: <https://doi.org/10.1007/s00500-019-04635-7>.
- [43] H. Chegini, R. Naha, A. Mahanti, M. Gong, and K. Passi. *IEEE Access*, **11** (2023):92660–92675. DOI: <https://doi.org/10.1109/ACCESS.2023.3307311>.